ChemistryOpen

Research Article
doi.org/10.1002/open.202200185

Chemistry Europe
European Chemical Societies Publishing

www.chemistryopen.org

Chemical Bonding in the Catalytic Platform Material $Ga_{1-x}Sn_xPd_2$

Alim Ormeci,[a] Emilie Gaudry,[b] Marc Armbrüster,[c] and Yuri Grin*[a]

The underlying reasons for the catalytic activity of $Ga_{1-x}Sn_xPd_2$ ($0 \leq x \leq 1$) in the semi-hydrogenation of acetylene are analyzed considering electronic structure and chemical bonding. Analysis of the chemical bonding shows pronounced charge transfer from the *p* elements to palladium and an unusual appearance of the Pd core basins at the surface of the QTAIM (quantum theory of atoms in molecules) atoms. The charge transfer supports the formation of the negatively charged palladium catalytic centers. Gallium-only-coordinated palladium atoms reveal a smaller effective charge in comparison with palladium species having tin in their coordination sphere. Within the empirical tight-binding approach, different influence of the *E*-Pd distances on the calculation matrix for the energy eigenvalues and the electronic density of states (DOS) leads to an S-like shape of the plot of the energy position of the 4*d* band center of gravity versus substitution level *x*. The latter correlates strongly with the catalytic activity and with the varying charge transfer to palladium. The optimal value of negative palladium charge and the closest position of Pd *d*-states gravity center towards the Fermi level correlates well with the catalytically most active composition *x*. Combination of all features of the chemical bonding and electronic structure allows more insight into the intrinsic reasons for the catalytic activity variation in the platform material $Ga_{1-x}Sn_xPd_2$ ($0 \leq x \leq 1$).

Introduction

The intermetallic compound $GaPd_2$, which started out as a component in dental amalgams,[1] has been developed into a platform material[2] for quite a number of catalytic reactions. These include the selective hydrogenation of acetylene, which is an important industrial process to clean the ethylene feed for the production of polyethylene (80×10^6 t/a[3]) or ethylene oxide (10×10^6 t/a[4]) in the gas phase[5–8] (also propyne[9]) and in the liquid phase,[10] furthermore in methanol steam reforming to release high-purity hydrogen from methanol/water mixtures,[12–15] and finally in the synthesis of methanol from CO[16] or CO_2,[16–22] as well as for the synthesis of dimethyl ether (DME) from CO and the electrocatalytic hydrogen evolution reaction[23] or methanol oxidation reaction.[24] The latter reactions, in particular, enable an efficient synthesis, or use of, methanol/DME as chemical storage molecules for a hydrogen-based energy infrastructure (*methanol economy*[25]).

Research on heterogeneous catalysis benefits from disentangling the electronic and structural effects as demonstrated in the case of the semi-hydrogenation of acetylene. Fine structural (geometric) effects can be studied by employing isostructural substitution of the main group metal by another main group metal with the same valence electron count.[26]

$GaPd_2$ is available as supported (see catalytic reports cited above as well as Ref. [27]) and unsupported nanoparticles[28] (and even as ink for printing[29]), thin films,[14,30] as bulk polycrystalline material[31] or in the form of large single crystals.[32] This impressive variety closes the materials gap and allows studying of the catalytic properties in electrocatalysis, in the gas and liquid phase as well as in surface science. Precise structural data for the bulk structure[31] as well as for the altered surface of $GaPd_2$ nanoparticles[33] are available, thus allowing modelling of catalytic paths by DFT-based calculations.[34]

Starting with the first publication of the phase diagram for the system Ga–Pd,[35,36] the $GaPd_2$ phase was reported to have a temperature-dependent homogeneity range with the width of several at.%. Nevertheless, usually only one set of the lattice parameters was supplied,[31,37,38] which did not allow to verify the existence of the homogeneity range. Also, during crystal structure refinement from both single crystal[31] and powder diffraction data,[39] no signs for mixed occupation of the positions were reported. Only later, the systematic change of lattice parameters ($a = 5.4762$–5.4252 Å, $b = 4.0570$–4.0684 Å, $c = 7.7973$–7.8813 Å), within the homogeneity range $Ga_{1-x}Pd_{2+x}$ ($0 \leq x \leq 0.17 + \delta$), was experimentally proven at 980 °C with additional Pd partially occupying the gallium position,[38] as

[a] *Dr. A. Ormeci, Prof. Y. Grin*
Max-Planck-Institut für Chemische Physik fester Stoffe
Nöthnitzer Str. 40
01187 Dresden (Germany)
E-mail: grin@cpfs.mpg.de
[b] *Prof. Dr. E. Gaudry*
Institut Jean Lamour
Université de Lorraine
2 al. André Guinier
54011 Nancy (France)
[c] *Prof. Dr. M. Armbrüster*
Faculty of Natural Sciences
Institute of Chemistry
Materials for Innovative Energy Concepts
Chemnitz University of Technology
09107 Chemnitz (Germany)

Supporting information for this article is available on the WWW under https://doi.org/10.1002/open.202200185

obtained from X-ray powder diffraction data. This is important, because the very recent observations show that the catalytic properties of a specific intermetallic compound with a significant homogeneity range can strongly depend on its composition. The intermetallic compound ZnPd is an impressive example for this, for which it has been shown that a concentration change of as little as 1 at.% is responsible for the abrupt reduction of the CO_2 selectivity in methanol steam reforming from 98% to only 10%.[40] Insights into the influence of the composition on the catalytic properties of Ga_2Pd are not yet available.

The interest in $GaPd_2$ as a catalytic material was increased even more by discovery, how the catalytic properties in the semi-hydrogenation of acetylene on the solid solution $Ga_{1-x}Sn_xPd_2$ ($0 \leq x \leq 1$) were influenced by electronic factors. Due to the only marginal changes in the crystal structure, the whole series shows excellent selectivity for ethylene, comparable with the binary $GaPd_2$, and a maximum of the specific catalytic activity around $x = 0.28$.[41] This finding attracted special attention to $SnPd_2$, the isotypic analogue of $GaPd_2$.

While it has been shown that $GaPd_2$ is stable *in operando*,[5] marked changes are observed under methanol steam reforming conditions, resulting in partial decomposition of the compound.[42] The latter behavior is detrimental when trying to connect the catalytic properties of intermetallic compounds to their crystal and electronic structures for enabling a knowledge-based development of heterogeneous catalysts.[2,43] The structural changes with composition as well as the chemical stability of the compound in reactive atmospheres are determined by the chemical behavior of the components which is mainly governed by the chemical bonding in the compound, a question which has not been addressed up to now.

While a lot is known about the EPd_2 (E = Ga, Sn) compounds (including enthalpies of formation,[44,45] the stability in different atmospheres[46] and the phase relations in the Ga–Sn–Pd system[47,48]), the issue of chemical bonding in the binary materials and, in particular, in the ternary solid solution, has been only scarcely addressed. The latter is responsible for the crystal and electronic structure, which defines the stability, adsorption and thus the catalytic properties. This study provides a quantum chemical analysis of the chemical bonding in $Ga_{1-x}Sn_xPd_2$ materials ($0 \leq x \leq 1$). The obtained results derive a sound description of the atomic interactions. This information forms the basis for a further understanding of the catalytic properties of $Ga_{1-x}Sn_xPd_2$ materials as well as their chemical behavior under reaction conditions.

Computational Details

First-principles electronic structure calculations for $GaPd_2$ and $SnPd_2$ were performed, using the crystallographic data,[31,49] within the local density approximation to the density functional theory using either the all-electron, full-potential local orbital method[50] (FPLO (version 9.01) or with the Fritz-Haber Institute ab initio molecular simulations method (FHI-aims).[51] Exchange and correlation effects were considered by employing the Perdew-Wang parametrization.[52] The number of irreducible k-points sampling the first Brillouin zone was 350, and the value of the maximum orbital angular momentum used in the expansion of the electron density was 12. Core states were treated using a fully-relativistic approach, while semi-core and valence states were treated at the scalar-relativistic level. The basis set consisted of Pd (4*s*, 4*p*+5*s*, 6*s*; 4*d*, 5*d*; 5*p*), Ga (3*s*, 3*p*, 3*d*+4*s*, 5*s*; 4*p*, 5*p*; 4*d*) and Sn (4*s*, 4*p*, 4*d*+5s, 6*s*, 5*p*, 6*p*, 4*d*) orbitals corresponding to semi-core+genuine valence states, respectively. In all FHI calculations, the first basis set and tight-binding settings for Pd, Sn and Ga were used.

The disordered cases corresponding to the compositions $x = {}^1/_6$, ${}^1/_4$, ${}^1/_3$, ${}^1/_2$, ${}^2/_3$ and ${}^3/_4$ were studied by constructing ordered models in the smallest possible unit cells (cf. Supporting Information item 1). The lattice parameters for each composition were chosen by interpolating the experimentally obtained data,[41] while the atomic positions were optimized according to maximum force criterion of 5.0 meV Å^{-1}. For the compositions with $x = {}^1/_4$, ${}^1/_2$ and ${}^3/_4$, the 12-atom unit cell (space group *P*1) was used, and the remaining cases were modeled with super cells of $3\times1\times1$, $1\times3\times1$ and $1\times1\times3$. The *d* band centers of gravity, ε^d_{cg}, were calculated from the projected density of Pd states (pDOS). For compositions with more than one inequivalent configuration, averages were computed by applying the Boltzmann factors as weights [Eq. (1)]:

$$< \varepsilon^d_{cg} > = (\Sigma_\sigma\, g_\sigma\, (\varepsilon^d_{cg})_\sigma\, e^{-E(\sigma)/kT})/Z \quad (1)$$

Here, $Z = (\Sigma_\sigma\, g_\sigma\, e^{-E(\sigma)/kT})$ is the partition function of the canonical ensemble with $E(\sigma)$ and g_σ being the total energy and multiplicity of a particular atomic configuration σ, respectively. Room temperature was taken for the temperature *T*.

Chemical bonding analysis was carried out within the electron localizability approach.[54,55] Both, electron localizability indicator ELI-D and electron density ED were calculated either with the specialized module in the FPLO,[56] or within the FHI-aims[53] packages. Topological analysis of ELI-D and ED was performed using the program DGrid.[57]

Results and Discussion

Crystal Structure

The EPd_2 intermetallic compounds $GaPd_2$ and $SnPd_2$ crystallize in the β-$CoSi_2$ type (space group *Pnma*, $a = 5.4829(8)$ Å; $b = 4.0560(4)$ Å, $c = 7.7863(8)$ Å for $GaPd_2$[31] and $a = 5.6424(2)$ Å; $b = 4.3072(1)$ Å, $c = 8.0899(3)$ Å for $SnPd_2$[49]). For the ternary solution $Ga_{1-x}Sn_xPd_2$, the lattice parameters increase monotonically with *x*. Thereby, the values of *a* and *c* show slightly positive, the values of *b* slightly negative deviation from linearity. The sum of all three results in the linear increase of the unit cell volume depending on *x*.[24,41]

Both binary crystal structures contain two different crystallographic positions for palladium and one for gallium or tin. For each position, the first coordination sphere is defined by a pronounced gap in the distances to the neighboring atoms around 3.0–3.1 Å, resulting in coordination of five gallium (tin) and eight palladium atoms for each palladium atom and ten palladium atoms for the *E* position (Figure 1).

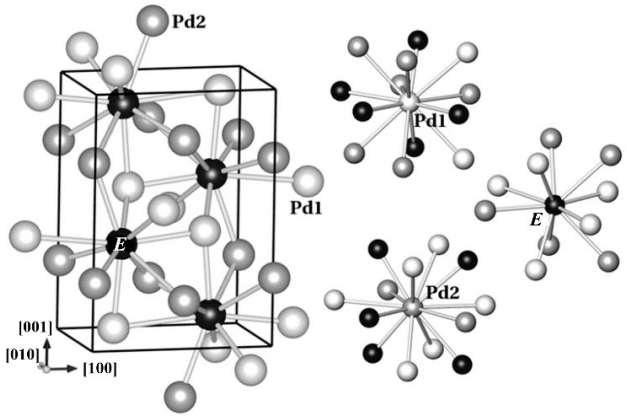

Figure 1. (left) Atomic arrangements in $GaPd_2$, $Ga_{1-x}Sn_xPd_2$ and $SnPd_2$ with the shortest E–Pd contacts (the unit cell is represented as a black box, *E* represents Ga, Sn and $Ga_{1-x}Sn_x$). (right) The atomic environments of *E*, Pd1 and Pd2.

Chemical Bonding and Electronic Structure

Concerning the heteroatomic neighborhood, each Pd1 atom has distorted tetrahedral coordination by four heteroatoms with distances varying between 2.54 Å and 2.56 Å (Ga) and between 2.60 Å and 2.74 Å (Sn). One additional Ga (Sn) atom is further away at a distance of 2.96 (Ga) or 3.01 Å (Sn). The environment of Pd2 is differentdistorted trigonal bipyramidal coordination by three Ga (Sn) atoms with *d*(Pd2–Ga) = 2.56–2.62 Å or *d*(Pd2–Sn) = 2.69–2.82 Å and two other Ga (Sn) atoms at considerably longer distances of 2.85 Å and 2.95 Å, respectively. The closest Pd–Ga and Pd–Sn contacts are comparable with the sum of covalent radii of Pd (1.28 Å), Ga (1.25 Å) and Sn (1.40 Å).[58] The coordination sphere of each palladium site is completed by eight Pd atoms with *d*(Pd–Pd) between 2.82 Å and 2.99 Å in $GaPd_2$ or between 2.87 Å and 3.08 Å in $SnPd_2$, thus completing the coordination number of both crystallographic positions to 13. These contacts are 2.5% to 12% longer than the interatomic distance of 2.75 Å in elemental Pd.[59] The *E* atoms are surrounded exclusively by ten palladium atoms. The shortest Ga–Ga and Sn–Sn distances of 3.43 Å and 3.61 Å, respectively, are significantly longer than the average interatomic distances of 2.70 Å and 3.10 Å in the α-modifications of Ga or Sn,[59] respectively. The environment of *E* atoms is formed by seven Pd atoms in the range of 2.54–2.62 Å and three Pd atoms at distances 2.85 Å (2×) and 2.96 Å (1×) for *E* = Ga and six Pd in the range of 2.62–2.69 Å and further four Pd atoms at distances from 2.82 Å to 3.01 Å for *E* = Sn. Despite Pd being a clear majority component, preference for heteroatomic interactions in the structure is indicated by analysis of interatomic distances, and, by taking similar observations for the intermetallic compounds GaPd[60] and Ga_2Ir[61] into account, can be considered as a driving force for the structures realized by the chemically similar compounds in the Ga–Pd and Sn–Pd systems.

While the bonding analysis based on the interatomic distances is coarse and, de facto, limited to two-center interactions only, the quantum chemical analysis in position space based on the electron localizability approach – combined analysis of electron-localizability indicator (ELI–D) and electron density (ED) – can provide information on a wider spectrum of interactions, from lone pairs to multi-center bonds.[54,55,62,63] In the distribution of ELI–D, one recognizes the individual core regions and the common valence region. For non-interacting atoms, the ELI–D distribution is spherically symmetric. Any deviation from spherical distribution indicates appearance of atomic interactions. The bonds are visualized by local ELI–D maxima (attractors) in the valence region.

The number of electrons in the basins (basin population) of these ELI–D bond attractors can be computed by integrating the electron density inside each bond basin. This procedure for the ELI–D is very similar to the one applied by R. Bader[64,65] to the electron density, which forms a part of his quantum theory of atoms in molecules (QTAIM). In the case of the ED, the attractors are usually located at nuclear sites and the corresponding basins are called atomic basins (QTAIM atoms). The electron population of the atomic basins can then be used to determine the effective charges of atoms and, further, the charge transfer. The intersection of an ELI–D bond basin with the participating atomic basins enables to compute how many electrons each atom contributes to the population of the respective bond basin.[66] This basin-intersection technique yields the number of atoms participating in a bond. Additional information on atomic interactions can be obtained by examining the ELI–D distribution in the penultimate shell.

The crystal structures of $GaPd_2$ and $SnPd_2$ are isotypic to $PbCl_2$ and dichlorides of alkaline-earth metals, which may suggest a pronounced ionic contribution to the bonding in EPd_2. Nevertheless, the shapes of the QTAIM atoms in both palladium compounds (Figure 2) already show that the bonding picture is more complex. Each QTAIM atom possesses several rather plane facets, characteristic for covalent bonding. The atomic shapes of symmetrically equivalent atoms in the gallium and tin EPd_2 compounds are very similar, concerning the number and the outline of the facets, being similar to those found in GaPd.[60] Integration of the electron density within QTAIM atoms reveals a charge transfer from Ga or Sn to Pd. The effective charges are practically independent of the calculation technique (Figure 2). The direction of the charge transfer agrees, in general, with electronegativity, according to which Pd is the more electronegative component (after Pauling:[67] Pd: 2.20; Ga: 1.60; Sn: 1.9). While the effective charge of palladium is in the range around −0.3 to −0.4, the effective charge of gallium is slightly smaller than that of tin, since tin has one more valence electron available, compared to gallium, to transfer to palladium. This follows rather the Sanderson (Ga: 2.4; Sn: 2.3[68]) and not the Pauling electronegativity and, in addition, influences the polarity of bond (cf. below). The study on the chemically related compound Ga_3Fe with more moderate charge transfer ($Fe^{0.32-}$, $Ga1^{0.10+}$, and $Ga2^{0.11+}$) employing the natural-domain-orbitals technique showed essential occupation of the 4*s* and 4*p* states of iron.[69] Considering even stronger charge transfer in Ga_2Pd and Sn_2Pd, the Pd 5*s* and – most probably – 5*p* states may be analogously essentially populated in these compounds. Pronounced charge transfer in Ga_2Pd

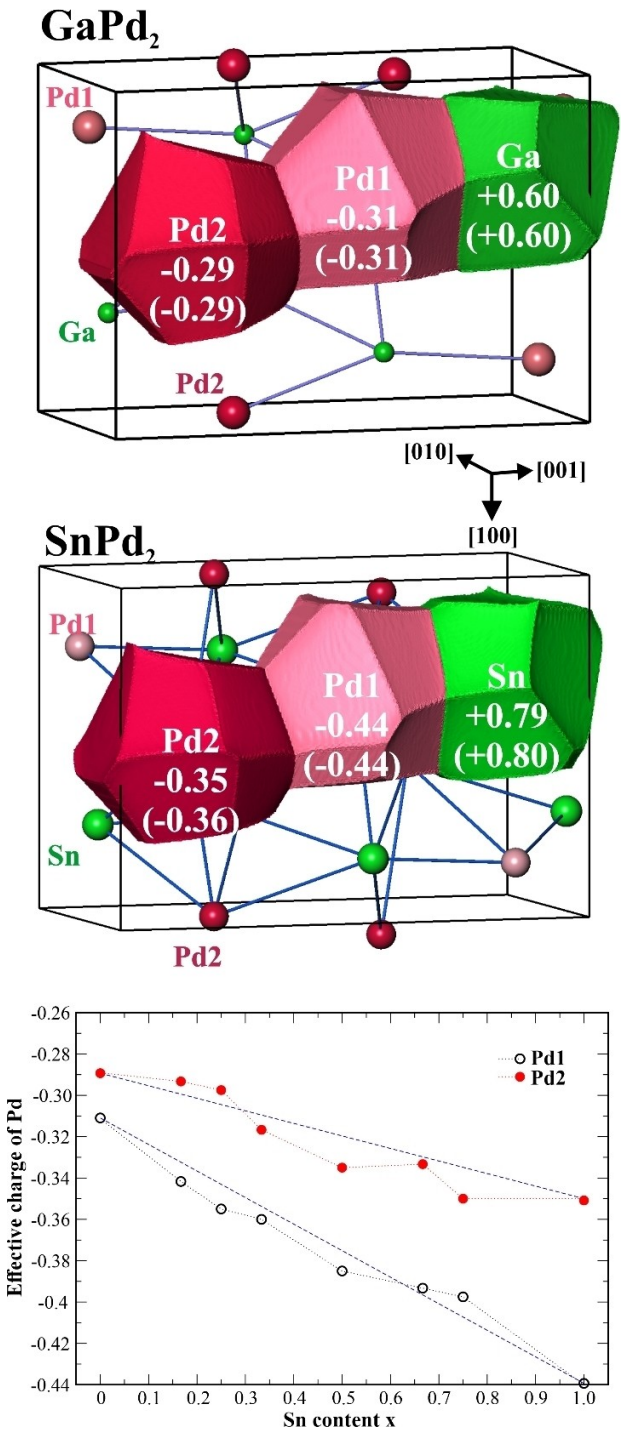

Figure 2. Upper and middle panels: QTAIM atomic shapes and charges in $GaPd_2$ and $SnPd_2$. For binary compounds: upper number – charge from the FHI-aims calculation, lower number in parenthesis – charge from the FPLO calculation. Bottom panel: Effective QTAIM charges of palladium in $Ga_{1-x}Sn_xPd_2$ in dependence of the tin content (FPLO calculations).

makes the formation of the homogeneity range by simple Pd/Ga substitution, as suggested in Ref. [38], rather unfavorable energetically. More complex mechanisms of homogeneity ranges, based on the embedding of compositionally and structurally different segments in the basic structural matrix (inhomogeneous intergrowth) should be considered. Such an approach was applied to the analysis of the Ga–Pd structures from the crystallographic point of view[70] and was recently experimentally confirmed for an example of the Laves phase $NbFe_2$.[71]

Since the adsorption of acetylene will most likely occur on the Pd atoms as in the case of GaPd,[53,72] the initial increase of the catalytic activity by adding tin[41] may have its origin in the charge transfer described above. In order to verify this assumption, the atomic charges were studied for different values of *x* (Figure 2, bottom panel), employing the lowest-energy structure for each composition (*x*) investigated. While the average QTAIM charges in the ternary solid solution follow the *x* values, the effective charges of the palladium atoms, which do not have Sn atoms in their coordination sphere are smaller than that with Sn atoms in the coordination, that is, addition of tin clearly regulates the effective charge of palladium. The average charge values for Pd atoms follow the lines connecting the end points with small fluctuations. They can be interpolated to get charge transfer/effective charges at any Sn content. Then, the dependence of the experimentally measured activities[41] on the total charge transfer to Pd per formula unit (Figure SI2) clearly shows an optimum charge transfer yielding maximum activity.

The assumption about the essential influence of the charge transfer, and thus on the position of the *d* band center, on the catalytic activity agrees also well with the similarity of the general bonding picture in $GaPd_2$ and $SnPd_2$ obtained by the ELI–D/ED intersection technique. The distribution of ELI–D in both compounds is similar to the one for GaPd.[60] While the inner shells of Ga and Sn reflect spherical symmetry, the penultimate (4^{th}) shell of Pd is structured in both compounds, indicating participation of these electrons in the bonding within the valence region. The structuring for Pd1 and Pd2 is different (Figure 3), which implies non-equivalent behavior of the 4d electrons and could result in different catalytic activity of the two sites.

Four types of bonding basins are common for both, $GaPd_2$ and $SnPd_2$ (red, orange, blue and pink in Figure 4). Most of them represent four- or five-atomic bonds with participation of one gallium or tin and three to four palladium atoms in each bond. As an example, the bond basins of the Ga–Pd2–Pd1–Pd1 and Sn–Pd2–Pd1–Pd1 (orange in Figure 4) has common surfaces with the ELI–D basins of inner shells (core basins) of the participating atoms and intersects with the according atomic (QTAIM) basins. The populations of bonding basins in EPd_2 compounds are very similar (Figure 4). Each bond basin has only one contribution from Ga (Sn), which is the largest individual one to the basin population. The total contribution of 2–4 participating palladium atoms is on average slightly larger than that of Ga in $GaPd_2$. Using the approach from Refs. [73,74], one can calculate the polar character for the basin *B* of such multiatomic bond as shown in Equation (2)

$$lpc = 2\frac{\sum_i (N_{Pd})_i}{N_B} - 1, \quad (2)$$

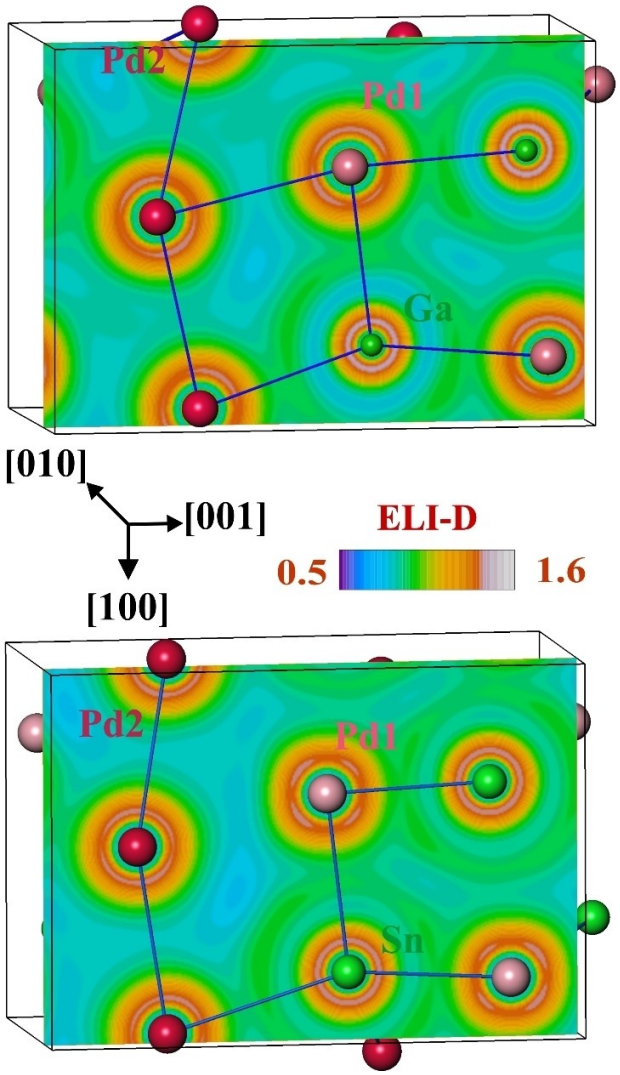

Figure 3. ELI–D distribution in the plane at $y = {}^{1}/_{4}$ in $GaPd_2$ (top) and $SnPd_2$ (bottom).

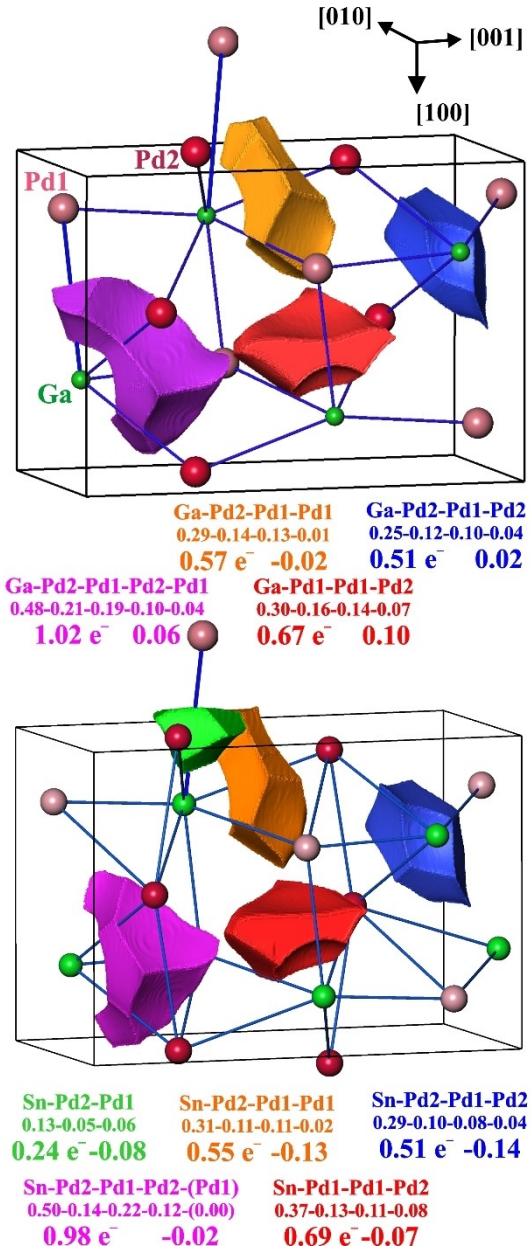

Figure 4. Multiatomic bonding in $GaPd_2$ (top) and $SnPd_2$ (bottom) shown by means of symmetry-independent ELI–D bonding basins and their populations (FPLO calculations). For each basin: first line – participating atoms, second line – the contributions of each participating atom to the basin population (in e^-), third line – bonding basin population (in e^-) and bond polarity after Refs. [73,74].

where N_B is the total population of the bond basin B, $(N_{Pd})_i$ is the contribution of the individual Pd atoms to the bond basin B. For the non-polar bond, the polarity calculated like above is 0, for the fully ionic case (or closed-shell configuration) *Ipc* is 1. If the *Ipc* value is negative, the considered atom does not contribute the larger part of the population. For multiatomic interactions in $GaPd_2$, one obtains relatively mild bond polarities between −0.02 and 0.10, that is, the bond polarity behaves along with the QTAIM charge transfer. In case of tin, the total contributions of participating palladium atoms to the bonding basins is smaller than the one of tin yielding the opposite polarities between −0.14 and −0.02. A similar tendency was recently found for Ga_2Pt and Sn_2Pt, where Sn contributes more electrons than Pt to the basin of the *E*-Pt bond (polarity of −0.34), while the Ga contribution is closer to but smaller than that of Pt (polarity of 0.18). This kind of behavior of tin in the bonding, in particular, the role of the number of valence electron available for bonding, is still under investigation.[75] An additional triatomic bond with a small basin population appears in $SnPd_2$ in FPLO calculations (0.24 e^-, green in Figure 3, bottom), obviously due to the increased number of valence electrons per unit cell.

In total, this analysis reveals very moderately polar multiatomic bonds with different directions of polarity for Ga and Sn, and results in small, but noticeable differences between $GaPd_2$ and $SnPd_2$, even if the rather small basin populations are taken into consideration. The bonding situation helps to explain the quite complex interconnection between the composition and

the catalytic activity of $Ga_{1-x}Sn_xPd_2$, which results in the observed 'volcano' plot.[41]

The similarities and the tiny differences in chemical bonding between $GaPd_2$ and $SnPd_2$ are also recognizable in the band structure. The calculated electronic densities of states (DOS) of both compounds are very similar and can be considered as consisting of three ranges (Figure 5). The low-energy range ($E \leq -7$ eV for $GaPd_2$ and $E \leq -8$ eV for $SnPd_2$) is formed by *s* states of the *E* component together with a small amount of Pd(*d*) states and reflects, in a general way, the bonding in both compounds. The remaining part shows two clear maxima at around −4 eV and −2 eV ($GaPd_2$) and ata −4.5 eV and −2.5 eV ($SnPd_2$). While the region around the first maximum ($-6\,eV < E < -3$ eV for $GaPd_2$ and $-7 < E \leq -3.5$ eV for $SnPd_2$) is formed by contributions of *E*(*p*), Pd(*s*) and Pd(*d*) states, mainly the Pd(*d*) states (with some admixture of *E*(*p*)) contribute to the DOS part below the Fermi level. A characteristic decrease of the total DOS near the Fermi level is observed for both intermetallic compounds $GaPd_2$ (0.45 states eV^{-1} $atom^{-1}$ at E_F) and $SnPd_2$ (0.39 states eV^{-1} $atom^{-1}$ at E_F).

In terms of the *d* bands, there is an optimum value for the distance of the *d* band center of gravity to the Fermi level which provides the suitable adsorption strength for the molecule and the surface involved in the reaction.[76] Following this approach, the examination of the Pd(*d*) contributions in the binary compounds shows the width of the highest-lying valence band, which is dominated by the *d* states, being 5.9 and 6.5 eV for $GaPd_2$ and $SnPd_2$, respectively. The centers of the Pd, Pd1-only and Pd2-only *d* bands are located at −3.02, −3.08 and −2.96 eV, respectively, for $GaPd_2$ with the corresponding values of −3.22, −3.33 and −3.10 eV for $SnPd_2$. According to the experimental data,[41] the catalytic activity of $GaPd_2$ is roughly 10 times higher than that of $SnPd_2$, indicating that Pd(*d*) band energies should not be too far from the Fermi level. The situation in the solid solution $Ga_{1-x}Sn_xPd_2$ may be interpreted in the simplest form of the rigid-band approximation,[77,78] assuming that the DOS remains constant and the Fermi level is adjusted according to the changed electron count. In the present case, it would mean that as Sn replaces Ga, the number of electrons will increase and therefore the Fermi level will move up. Since the *d* bands remain unchanged (rigid) upon substitution, their band centers should also remain the same. However, their distance to the Fermi level will increase due to the change in Fermi level position. This scenario yields a monotonic change of the *d* band center as a function of Sn content, and thus cannot explain the behavior of the experimentally observed catalytic activity of the $Ga_{1-x}Sn_xPd_2$ materials, in particular the maximum activity measured at the nominal composition of $x = 0.28$.[41] As each Sn substitution will increase the number of electrons in the unit cell, the Fermi level will accordingly keep moving up and would, within the rigid-band approach, result in a linear decrease of the *d* band center position from −3.02 to −3.22 eV. Therefore, it is clear that Sn substitution modifies the atomic interactions in a non-trivial and composition-dependent way. To understand these changes, the electronic structure features were investigated in various super-cell models with different compositions, namely, with x = $^1/_6$, $^1/_4$, $^1/_3$, $^1/_2$, $^2/_3$ and $^3/_4$. The variation of the total Pd *d* band center position with *x* reveals an S-like shape containing a maximum at around $x = 0.25$ and a minimum at x→1 (Figure 6, top), which is also observed for the according *d* band gravity centers' positions of Pd1 and Pd2 (Figure 6, bottom). The Pd1 atom has four *E* = Ga/Sn neighbors as the shortest contacts compared to three *E*–Pd contacts for the Pd2 atoms (Table SI3). This may imply that Pd1–*E* interactions are stronger than Pd2–*E*, which results in lower energies for Pd1 *d* band centers which are 0.12–0.23 eV below those of the Pd2 atoms.

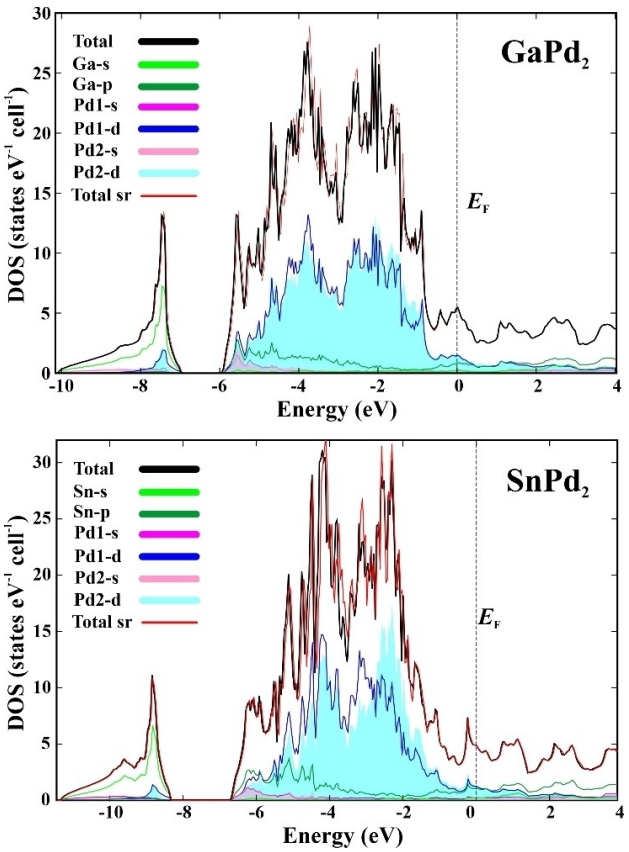

Figure 5. Electronic density of states (DOS) of $GaPd_2$ and $SnPd_2$ (fully-relativistic approximation) with partial contributions of the relevant atomic states and total density of states in semi-relativistic approximation for comparison (red).

The failing of the rigid-band approach in the pseudo-binary system $Ga_{1-x}Sn_xPd_2$ can be understood within the empirical tight-binding (ETB) method. The electronic DOS is calculated from the energy eigenvalues obtained by diagonalizing a matrix at numerous k points. In the ETB approximation this matrix is the Hamiltonian containing the off-diagonal matrix elements *V*(A,l;B,l') evaluated between the atomic orbitals l and l' of the atoms A and B.[79,80] The magnitude of *V*, in general, depends inversely on the interatomic distance d_{AB}. If d_{AB} increases, $|V|$ decreases, and vice versa. Values of the matrix elements *V*(Pd;Ga) and *V*(Pd;Sn) in the binary compounds $GaPd_2$ and $SnPd_2$, respectively, can be taken as reference or optimum values, because they are evaluated at the equilibrium volume (implying optimum interatomic distances). In the solid solution $Ga_{1-x}Sn_xPd_2$, with small *x* values, the crystal structure refinements

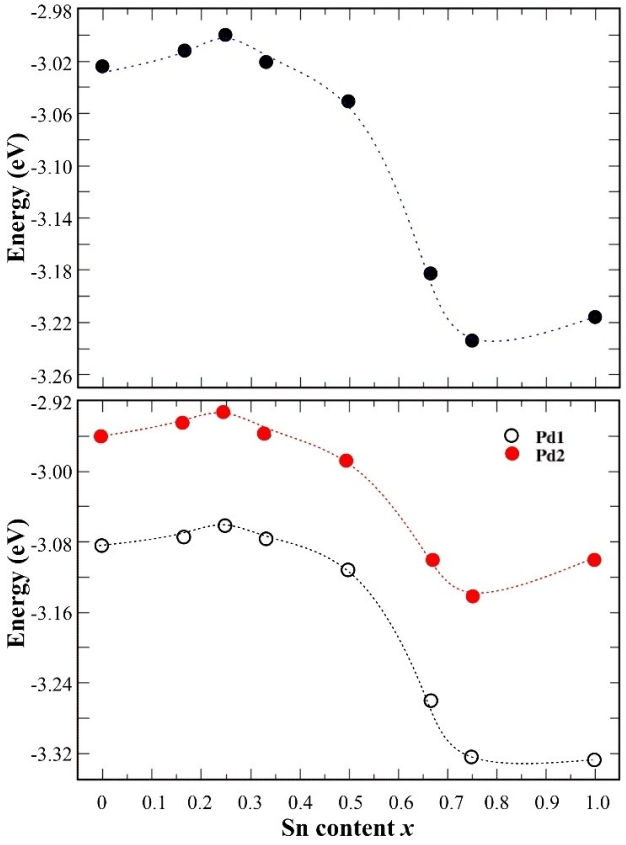

Figure 6. Energy position of the 4*d* band gravity center in the electronic DOS for $Ga_{1-x}Sn_xPd_2$ (optimized structure models) versus *x*: (top) gravity center position of the combined Pd1 + Pd2 4*d* band; (bottom) position of the Pd1- and Pd2-4*d* band gravity centers. Dashed lines are guides for the eye only.

cannot resolve the local positions of Ga and Sn atoms occupying the same Wyckoff site. Consequently, identical averaged coordinates and thus identical Ga–Pd and Pd–Sn distances have to be considered in first approximation.

The unit cell volume of the pseudo-binary system $Ga_{1-x}Sn_xPd_2$ increases linearly, when Sn substitutes Ga; thus Ga–Pd interatomic distances become longer, $|V(Pd;Ga)|$ values get smaller, and these smaller values imply that the *d* states move closer to the Fermi level. At the same time, however, Pd–Sn distances for small *x* are much shorter than the optimum Pd–Sn distances of $SnPd_2$, causing larger $|V(Pd;Sn)|$ values. The latter matrix elements will act in the opposite direction, driving the *d* states to lower energies farther away from the Fermi level. For small *x* values, there will be many more *V*(Pd;Ga) than *V*(Pd;Sn) terms with the net effect that the *d* band center is pushed up towards the Fermi level. As *x* increases further, the competition between these two counteracting effects will evolve smoothly, with the *d* band center position first rising up until some maximum, then start decreasing. Similar reasoning applies to the other end with *x* being decreased starting from 1.0, and it suggests the existence of a minimum. Since the maximum and minimum are expected to occur away from the end points 0.0 and 1.0, the shape of the *d* band center versus *x* curve should look like an 'S'. An additional contributor is, of course, the fact that the Fermi level itself will move up as *x* changes from 0 to 1 to accommodate the extra electrons due to the Sn contribution. Consequently, the actual Sn content, at which the maximum and minimum of the *d* band center occur, will be determined by a combination of all three effects.

The $1\times1\times3$ supercell calculations carried out to simulate the $x = {}^1/_6$ model provide a good example to support the above considerations. The unit cell of this particular case contains six different Wyckoff positions for Pd1 and Pd2 (crystallographic details are given in the Supporting Information). Three of these for each Pd1 and Pd2 have no Sn atoms in their first coordination spheres. The calculated energy values for their *d* band centers are −3.01, −3.05 and −3.06 eV for Pd1, and −2.92, −2.88 and −2.93 eV for Pd2. The corresponding values for the other three positions having one or two Sn atoms in their first coordination sphere are −3.09, −3.11, −3.12 eV for Pd1, and −2.97, −3.01 and −2.96 eV for Pd2, respectively. It is clearly seen that, with respect to $GaPd_2$ (−3.08 and −2.96 eV), the *d* band centers of the 'no-Sn neighbor' Pd atoms shift closer to the Fermi level whereas those of the 'Sn-neighbor'-having Pd atoms move in the other direction. The averages for Pd1 and Pd2 are obtained as −3.07 and −2.94 eV, that is, the net effect is a slight upward shift.

Catalytic Activity versus Chemical Bonding and Electronic Structure

The bonding analysis reveals moderately polar multi-atomic heteroatomic bonds regularly (homogeneously) distributed in the unit cell. No planes especially suitable for preferential cleavage (i.e., separated by clearly weaker bonds) can be recognized. Thus, any random cleavage should lead to the appearance of the catalytically active Pd centers on the surface. Moreover, due to the higher Pd content, such centers may be formed by more than one Pd atom, that is, creating distinct conditions for the adsorption of acetylene molecules, which correlates with the higher catalytic selectivity of $Ga_{1-x}Sn_xPd_2$ in comparison with other Ga–Pd compounds.[3,24]

From the above analysis one may also recognize that the charge transfer and the *d* states of Pd crucially influence the catalytic activity of $Ga_{1-x}Sn_xPd_2$ materials. In the position space representation, this finds an additional rather unusual visualization in the relation between the QTAIM atomic shapes and ELI–D core shapes (Figure 7).

While the core shapes of the *E* components are spherical and completely embedded within the respective QTAIM shapes with relatively large distance to the QTAIM atoms borders, the core shapes of both palladium species are irregular. They are much closer to the border of the QTAIM shapes than in case of the *E* species and even partially cross borders of the respective QTAIM shapes (cf. black circles Figure 7), that is, the electrons of the penultimate shells (*d* electrons among others) of Pd are essentially more spatially accessible for the interactions, being on the surface of the material, than that of Ga or Sn. This allows the construction of the following hypothetical scenario for the catalytic behavior during the hydrogenation of acetylene. The

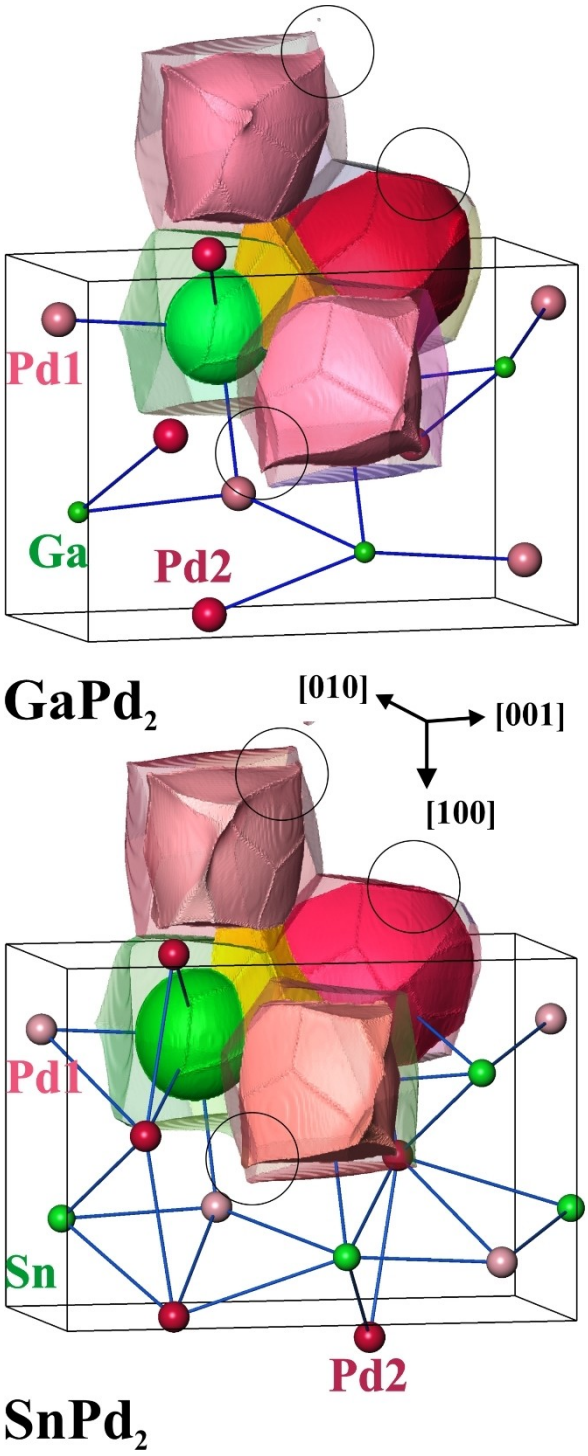

Figure 7. QTAIM atoms (transparent shapes) and ELI–D basins of the inner shells (pink and red basins) in $GaPd_2$ and $SnPd_2$ by formation of the four-atomic bonds Ga–Pd2–Pd1–Pd1 and Sn–Pd2–Pd1–Pd2 (orange bond basin, cf. Figure 4). For black circles, cf. text.

palladium species appearing on the surface of the material due to the random cleavage may function as adsorption centers for the acetylene and hydrogen molecules. Similar behavior is observed for the palladium species in GaPd, attracting the carbon atoms of the CO molecules during adsorption by the Coulomb interaction of the positively charged C atom (+1.2) and the negatively charged palladium atom (−0.4) according to the QTAIM analysis.[53] The difference in the effective charge and the local environment between the Pd1 and Pd2 positions may make them suitable for different adsorption sites, one for acetylene and one for hydrogen. The energetics of such interactions on the surface is of course dependent on the energy of the *d* states, which should be optimal. These features, in total, allow more insight into the catalytic behavior of $GaPd_2$, $SnPd_2$ and the solid solution $Ga_{1-x}Sn_xPd_2$ from the point of view of chemical bonding in solids. Further information about the mechanism of catalysis may be expected from the study of the catalytic behavior of the materials' surface, which is an ongoing project.

Conclusions

Position-space analysis of chemical bonding and electronic structure of the platform material $Ga_{1-x}Sn_xPd_2$ shows three striking features:

i) pronounced charge transfer from the *p* elements to palladium;
ii) unusual appearance of the core basins in the position-space representation of bonding;
iii) non-linear behavior of the center of gravity of the *d* states of palladium in the electronic density of states with the substitution level *x* in $Ga_{1-x}Sn_xPd_2$.

The position of the *d* band gravity center strongly correlates with the catalytic activity and seems to have an optimal value at around $x = 0.25$. Palladium atoms with a gallium-only environment reveal a smaller effective charge in comparison to the palladium species having tin in their coordination sphere. While partial (and local) increase of negative palladium charge positively influences the *d* states, with their center of gravity shifting towards the Fermi level, palladium species with only tin ligands (and the highest effective charge) have their d-states center of gravity further away from the Fermi level. This leads to a S-like shape of the plot of energy position of the *d* band gravity center versus the substitution grade *x* and allows understanding of the variation of catalytic activity for $Ga_{1-x}Sn_xPd_2$ on the atomic level.

Acknowledgements

Yu. G. and M. A. are grateful for the support of the Deutsche Forschungsgemeinschaft (grants GR 1793/19-1 and AR 617/14-1, respectively). Fruitful discussions with Frank R. Wagner, Miroslav Kohout and William P. Clark are kindly appreciated. The authors acknowledge the fruitful cooperation within the European Integrated Centre for Development of Alloys and Compounds (European CMAC).

Conflict of Interest

The authors declare no conflict of interest.

Data Availability Statement

The data that support the findings of this study are available from the corresponding author upon reasonable request.

Keywords: chemical bonding · electron-localizability approach · ELI–D · $GaPd_2$ · $SnPd_2$

[1] K. Hisatsune, K. Baba, M. Hasaka, T. Morimura, Y. Tanaka, K. Udoh, K. Yasuda, *J. Alloys Compd.* **1995**, *230*, 94–99.
[2] M. Armbrüster, *Sci. Technol. Adv. Mater.* **2020**, *21*, 303–322.
[3] O. G. Piringer, A. L. Baner, *Plastic Packaging: Interactions with Food and Pharmaceuticals*, 2nd ed., Wiley-VCH NY, **2008**, p. 1 ff.
[4] K. Weissermel, H.-J. Arpe, *Industrial Organic Chemistry*, 4th ed.; Wiley-VCH NY, **2003**, p. 1 ff.
[5] M. Armbrüster, K. Kovnir, M. Behrens, D. Teschner, Yu. Grin, R. Schlögl, *J. Am. Chem. Soc.* **2010**, *132*, 14745–14747.
[6] M. Armbrüster, M. Behrens, F. Cinquini, K. Fottinger, Yu. Grin, A. Haghofer, B. Klotzer, A. Knop-Gericke, H. Lorenz, A. Ota, S. Penner, J. Prinz, C. Rameshan, Z. Revay, D. Rosenthal, N. Rupprechter, P. Sautet, R. Schlögl, L. D. Shao, L. Szentmiklosi, D. Teschner, D. Torres, R. Wagner, R. Widmer, G. Wowsnick, *ChemCatChem* **2012**, *4*, 1048–1063.
[7] R. R. Zimmermann, T. Hahn, W. Reschetilowski, M. Armbrüster, *ChemPhysChem* **2017**, *18*, 2517–2525.
[8] A. Ota, M. Armbrüster, M. Behrens, D. Rosenthal, M. Friedrich, I. Kasatkin, F. Girgsdies, W. Zhang, R. Wagner, R. Schlögl, *J. Phys. Chem. C* **2011**, *115*, 1368–1374.
[9] M. Bauer, R. Schoch, L. D. Shao, B. S. Zhang, A. Knop-Gericke, M. Willinger, R. Schlögl, D. Teschner, *J. Phys. Chem. C* **2012**, *116*, 22375–22385.
[10] D. V. Glyzdova, N. S. Smirnova, N. N. Leont'eva, E. Y. Gerasimov, I. P. Prosvirin, V. I. Vershinin, D. A. Shlyapin, P. G. Tsyrul'nikov, *Kinet. Catal.* **2017**, *58*, 140–146.
[11] G. Wowsnick, D. Teschner, M. Armbrüster, I. Kasatkin, F. Girgsdies, Yu. Grin, R. Schlögl, M. Behrens, *J. Catal.* **2014**, *309*, 221–230.
[12] H. Lorenz, S. Penner, W. Jochum, C. Rameshan, B. Klotzer, *Appl. Catal. A* **2009**, *358*, 203–210.
[13] C. Rameshan, H. Lorenz, M. Armbrüster, I. Kasatkin, B. Klotzer, T. Gotsch, K. Ploner, S. Penner, *Catal. Lett.* **2018**, *148*, 3062–3071.
[14] L. Mayr, H. Lorenz, M. Armbrüster, S. A. Villaseca, Y. Luo, R. Cardoso, U. Burkhardt, D. Zemlyanov, M. Haevecker, R. Blume, A. Knop-Gericke, B. Klotzer, S. Penner, *J. Catal.* **2014**, *309*, 231–240.
[15] A. Haghofer, D. Ferri, K. Fottinger, G. Rupprechter, *ACS Catal.* **2012**, *2*, 2305–2315.
[16] L. D. Li, B. S. Zhang, E. Kunkes, K. Fottinger, M. Armbrüster, D. S. Su, W. Wei, R. Schlögl, M. Behrens, *ChemCatChem* **2012**, *4*, 1764–1775.
[17] R. Manrique, L. Rodriguez-Pereira, S. A. Rincon-Ortiz, J. J. Bravo-Suarez, V. G. Baldovino-Medrano, R. Jimenez, A. Karelovic, *Catal. Sci. Technol.* **2020**, *10*, 6644–6658.
[18] P. P. Wu, J. Zaffran, D. Y. Xu, B. Yang, *J. Phys. Chem. C* **2020**, *124*, 15977–15987.
[19] E. M. Fiordaliso, I. Sharafutdinov, H. W. P. Carvalho, J. Kehres, J. D. Grunwaldt, I. Chorkendorff, C. D. Damsgaard, *Sci. Technol. Adv. Mater.* **2019**, *20*, 521–531.
[20] K. Ahmad, S. Upadhyayula, *Sci. Technol.* **2019**, *9*, 529–538.
[21] A. Garcia-Trenco, E. R. White, A. Regoutz, D. J. Payne, M. S. P. Shaffer, C. K. Williams, *ACS Catal.* **2017**, *7*, 1186–1196.
[22] O. Oyola-Rivera, M. A. Baltanas, N. Cardona-Martinez, *J. CO_2 Util.* **2015**, *9*, 8–15.
[23] S. C. Lim, C. Y. Chan, K. T. Chen, H. Y. Tuan, *Nanoscale* **2019**, *11*, 8518–8527.
[24] R. Zerdoumi, O. Matselko, L. Rößner, Yu. Grin, M. Armbrüster, *J. Am. Chem. Soc.* **2022**, *144*, 8379–8388.
[25] G. A. Olah, G. K. S. Prakash, A. Goeppert, *J. Am. Chem. Soc.* **2011**, *133*, 12881–12898.
[26] Y. Luo, S. A. Villaseca, M. Friedrich, D. Teschner, A. Knop-Gericke, M. Armbrüster, *J. Catal.* **2016**, *338*, 265–272.
[27] M. Schmidt, K. Kovnir, J. Deichsel, M. Binnewies, Yu Grin, M. Armbrüster, *Z. Anorg. Allg. Chem.* **2015**, *641*, 1061–1068.
[28] M. Armbrüster, G. Wowsnick, M. Friedrich, M. Heggen, R. Cardoso-Gil, *J. Am. Chem. Soc.* **2011**, *133*, 9112–9118.
[29] M. Siebert, R. R. Zimmermann, M. Armbrüster, R. Dittmeyer, *ChemCatChem* **2017**, *9*, 3733–3742.
[30] R. R. Zimmermann, M. Siebert, S. Ibrahimkutty, R. Dittmeyer, M. Armbrüster, *Z. Anorg. Allg. Chem.* **2020**, *646*, 1218–1226.
[31] K. Kovnir, M. Schmidt, C. Waurisch, M. Armbrüster, Y. Prots, Yu. Grin, *Z. Kristallogr. New Cryst. Struct.* **2008**, *223*, 7–8.
[32] J. Schwerin, D. Muller, S. Kiese, P. Gille, *J. Cryst. Growth* **2014**, *401*, 613–616.
[33] R. Leary, F. de la Pena, J. S. Barnard, Y. Luo, M. Armbrüster, J. M. Thomas, P. A. Midgley, *ChemCatChem* **2013**, *5*, 2599–2609.
[34] M. Krajci, J. Hafner, *J. Phys. Chem. C* **2014**, *118*, 12285–12301.
[35] K. Schubert, H. L. Lukas, H.-G. Meissner, S. Bhan, *Z. Metallkd.* **1959**, *50*, 534–540.
[36] K. Khalaff, K. Schubert, *J. Less-Common Met.* **1974**, *37*, 127–140.
[37] K. Schubert, H. Breimer, W. Burkhardt, E. Günzel, R. Haufler, H. L. Lukas, H. Vetter, J. Wegst, M. Wilkens, *Naturwissenschaften* **1957**, *44*, 229–230.
[38] C. Wannek, B. Harbrecht, *J. Alloys Compd.* **2001**, *316*, 99–106.
[39] H. Kohlmann, *J. Solid State Chem.* **2010**, *183*, 367–372.
[40] M. Friedrich, D. Teschner, A. Knop-Gericke, M. Armbrüster, *J. Catal.* **2012**, *285*, 41–47.
[41] O. Matselko, R. R. Zimmermann, A. Ormeci, U. Burkhardt, R. Gladyshevskii, Yu. Grin, M. Armbrüster, *J. Phys. Chem. C* **2018**, *122*, 21891–21896.
[42] A. Haghofer, K. Föttinger, F. Girgsdies, D. Teschner, A. Knop-Gericke, R. Schlögl, G. Rupprechter, *J. Catal.* **2012**, *286*, 13–21.
[43] K. Kovnir, M. Armbrüster, D. Teschner, T. V. Venkov, F. C. Jentoft, A. Knop-Gericke, Yu. Grin, R. Schlögl, *Sci. Technol. Adv. Mater.* **2007**, *8*, 420–427.
[44] S. V. Meschel, O. J. Kleppa, *Thermochim. Acta* **1997**, *292*, 13–17.
[45] D. El Allam, M. Gaune-Escard, J. P. Bros, E. Hayer, *Metall. Trans. B* **1992**, *23*, 39–44.
[46] G. Wowsnick, D. Teschner, I. Kasatkin, F. Girgsdies, M. Armbrüster, A. P. Zhang, Yu. Grin, R. Schlögl, M. Behrens, *J. Catal.* **2014**, *309*, 209–220.
[47] O. Matselko, Yu. Grin, R. Gladyshevskii, U. Burkhardt, *Mat. Charact.* **2019**,*147*, 443–452.
[48] O. Matselko, U. Burkhardt, Yu. Prots, R. R. Zimmermann, M. Armbrüster, R. Gladyshevskii, Yu. Grin, *Eur. J. Inorg. Chem.* **2017**, *29*, 3542–3550.
[49] A. Götze, J. M. Sander, H. Kohlmann, *Z. Naturforsch. B* **2016**, *71*, 503–508.
[50] K. Koepernik, H. Eschrig, *Phys. Rev. B* **1999**, *59*, 1743.
[51] V. Blum, R. Gehrke, F. Hanke, P. Havu, V. Havu, X. Ren, K. Reuter, M. Scheffler, *Comp. Phys. Commun.* **2009**, *180*, 2175–2196.
[52] J. P. Perdew, Y. Wang, *Phys. Rev. B* **1992**, *45*, 13244.
[53] S. A. Villaseca, A. Ormeci, S. V. Levchenko, R. Schlögl, Y. Grin, M. Armbrüster, *ChemPhysChem* **2017**, *18*, 334–337.
[54] M. Kohout, *Int. J. Quantum Chem.* **2004**, *97*, 651–658.
[55] M. Kohout, F. R. Wagner, Yu. Grin, *Int. J. Quantum Chem.* **2006**, *106*, 1499–1507.
[56] A. Ormeci, H. Rosner, F. R. Wagner, M. Kohout, Yu. Grin, *J. Phys. Chem. A* **2006**, *110*, 1100–1105.
[57] M. Kohout, *DGrid*, versions 4.6–5.0, 2018–2021.
[58] J. Emsley, *The Elements*, Clarendon Press-Oxford University Press-NY, 3rd Ed. **1998**, p. 76 ff.
[59] J. Donohue, *Structure of the Elements*, John Wiley & Sons, New York, **1974**, p. 216 ff.
[60] Yu. Grin, M. Armbrüster, A. I. Baranov, K. Finzel, M. Kohout, A. Ormeci, H. Rosner, F. R. Wagner, *Mol. Phys.* **2016**, *114*, 1250–1259.
[61] M. Boström, Yu. Prots, Yu. Grin, *Solid State Sci.* **2004**, *6*, 499–503.
[62] F. R. Wagner, V. Bezugly, M. Kohout, Yu. Grin, *Chem. Eur. J.* **2007**, *13*, 5724–5741.
[63] F. R. Wagner, M. Kohout, Yu. Grin, *J. Phys. Chem. A* **2008**, *112*, 9814–9828.
[64] R. F. W. Bader, *Chem. Rev.* **1991**, *91*, 893–928.
[65] R. F. W. Bader, *Atoms in Molecules, A Quantum Theory*, Clarendon Press – Oxford University Press, NY, **1994**, p. 1 ff.
[66] S. Raub, G. Jansen, *Theor. Chem. Acc.* **2001**, *106*, 223–232.

[67] L. Pauling, *The Nature of the Chemical Bond and the Structure of Molecules and Crystals*, 3rd ed. Cornell University Press, Ithaca, **1960**, p. 88 ff.
[68] R. T. Sanderson, *J. Am. Chem. Soc.* **1983**, *105*, 2259–2261.
[69] F. R. Wagner, R. Cardoso-Gil, B. Boucher, M. Wagner-Reetz, J. Sichelschmidt, P. Gille, M. Baenitz, Yu. Grin, *Inorg. Chem.* **2018**, *57*, 12908–12919.
[70] Yu. Grin, In: E. Parthé (ed.) *Modern Perspectives in Inorganic Crystal Chemistry*. Kluver Academic Publishers, **1992**, p. 77–95.
[71] M. Šlapáková, A. Zendegani, C. H. Liebscher, T. Hickel, J. Neugebauer, T. Hammerschmidt, A. Ormeci, Yu. Grin, G. Dehm, K. S. Kumar, F. Stein, *Acta Mater.* **2020**, *183*, 362–376.
[72] J. Prinz, C. Pignedoli, Q. Stöckl, M. Armbrüster, H. Brune, O. Gröning, R. Widmer, D. Passerone, *J. Am. Chem. Soc.* **2014**, *136*, 11792–11798.
[73] D. Bende, F. R. Wagner, Yu. Grin, *Inorg. Chem.* **2015**, *54*, 3970–3978.
[74] F. R. Wagner, D. Bende, Yu. Grin, *Dalton Trans.* **2016**, *45*, 3236–3243.
[75] A. M. Barrios Jiménez, A. Ormeci, U. Burkhardt, S. G. Altendorf, F. Kaiser, I. Veremchuk, G. Auffermann, Yu. Grin, I. Antonyshyn, *Sustain. Energy Fuels* **2021**, *5*, 5762–5772.
[76] T. Bligaard, J. K. Nørskov, *Electrochim. Acta* **2007**, *52*, 5512–5516.
[77] E. A. Stern, *Phys. Rev.* **1967**, *157*, 544–551.
[78] M. S. Lee, S. D. Mahanti, *Phys. Rev. B* **2012**, *85*, 165149.
[79] W. A. Harrison, *Elementary Electronic Structure*, World Scientific, Singapore, **1999**, p. 11–32.
[80] J. C. Slater, G. F. Koster, *Phys. Rev.* **1954**, *94*, 1498–1524.

Manuscript received: August 18, 2022
Revised manuscript received: November 9, 2022